An experimental-nonlinear finite element study of a balloon expandable stent inside a realistic stenotic human coronary artery to investigate plaque and arterial wall injury

Article *in* Biomedizinische Technik/Biomedical Engineering · April 2015

DOI: 10.1515/bmt-2014-0144 · Source: PubMed

CITATIONS
14

READS
283

4 authors, including:

Reza Razaghi
University of Tabriz
43 PUBLICATIONS **495** CITATIONS
SEE PROFILE

Ahmad Shojaei
Basir Eye Center
36 PUBLICATIONS **646** CITATIONS
SEE PROFILE

Mahdi Navidbakhsh
Iran University of Science and Technology
143 PUBLICATIONS **2,423** CITATIONS
SEE PROFILE

Alireza Karimi, Reza Razaghi, Ahmad Shojaei and Mahdi Navidbakhsh*

An experimental-nonlinear finite element study of a balloon expandable stent inside a realistic stenotic human coronary artery to investigate plaque and arterial wall injury

Abstract: The stresses induced within plaque tissues and arterial layers during stent expansion inside an atherosclerotic artery can be exceeded from the yield stresses of those tissues and, consequently, lead to plaque or arterial wall rupture. The distribution and magnitude of the stresses in the plaque-artery-stent structure might be distinctly different for different plaque types. In this study, the mechanical properties of six healthy and atherosclerotic human coronary arteries were determined for application in plaque and arterial vulnerability assessment. A nonlinear finite element simulation based on an Ogden material model was established to investigate the effect of plaque types on the stresses induced in the arterial wall during implantation of a balloon expandable coronary stent. The atherosclerotic artery was assumed to consist of a plaque and normal arterial tissues on its outer side. The results indicated a significant influence of plaque types on the maximum stresses induced within the plaque wall and arterial wall during stenting but not when computing maximum stress on the stent. The stress on the stiffest calcified plaque wall was 3.161 MPa, whereas cellular and hypocellular plaques showed relatively less stress on their wall. The highest von Mises stresses within the arterial wall were observed on the hypocellular plaque, whereas the lowest stresses were seen to be located in the calcified and cellular plaques. Although the computed stresses on the arterial wall for the calcified and cellular plaques were not high enough to invoke a rupture, the stress on the hypocellular plaque was relatively higher than that of the strength of the arterial wall. These findings may have implications not only for understanding the stresses induced in plaque and the arterial wall, but also for developing surgeries such as balloon-angioplasty and stenting.

Keywords: arterial injury; atherosclerosis; coronary artery; nonlinear finite element simulation; plaque vulnerability.

DOI 10.1515/bmt-2014-0144
Received October 28, 2014; accepted March 11, 2015

***Corresponding author: Mahdi Navidbakhsh,** School of Mechanical Engineering, Iran University of Science and Technology, Tehran 16846, Iran; and Tissue Engineering and Biological Systems Research Laboratory, School of Mechanical Engineering, Iran University of Science and Technology, Tehran 16887, Iran, Phone: +98 21 77209027, Fax: +98 21 73021585, E-mail: mnavid@iust.ac.ir
Alireza Karimi and Reza Razaghi: School of Mechanical Engineering, Iran University of Science and Technology, Tehran 16846, Iran, and Tissue Engineering and Biological Systems Research Laboratory, School of Mechanical Engineering, Iran University of Science and Technology, Tehran 16887, Iran
Ahmad Shojaei: Department of Ophthalmology, Baqiyatallah University of Medical Sciences, Tehran 19945, Iran and Research Department, Basir Eye Center, Tehran 14186, Iran

Introduction

Atherosclerosis arises when additional cholesterol attaches itself to the walls of the blood vessels. It is ranked within the top deadliest cardiovascular diseases, in which embedded cholesterol attracts cellular waste products, calcium, and fibrin [27, 46]. These plaques can cause artery occlusion leading to a remarkable reduction in blood flow [8, 22].

Several treatment procedures are recommended to support the arterial walls to diminish the obstruction of arteries due to plaque occlusion, including balloon angioplasty and stenting, bypass surgery, and atherectomy [1, 50]. In cases of coronary artery occlusion, most percutaneous treatment procedures involve coronary stent implantation, which is a mechanical method for coronary artery disease treatment. The outcomes of stenting procedures depend on the geometry and the mechanical properties of each component involved in this process, that is, the artery, plaque, stent, and balloon [2].

Plaques are histologically classified as calcified, cellular, and hypocellular, which have been shown to have statistically different mechanical properties under radial

compressive loading [41], and non-significant differences under tensile loading [44]. Although it has been reported that the stiffness of hypocellular plaques were on average about twice as stiff as cellular plaques under tensile stress, statistical analyses revealed non-significant alterations within the tensile properties of plaque groups. Therefore, it might be expected that different plaques respond differently to the same stenting procedure [52]. As it has been shown that plaque type can be determined using imaging techniques [4, 47], quantifying the injury or loading within different plaques and arterial wall during stenting is necessary to determine the magnitude of stresses and, consequently, optimize both stenting procedures and the design of stents.

The finite element (FE) method has been used extensively to investigate implant-artery interactions during and following stent placement [11, 38, 43, 54]. Finite element models of complex atherosclerotic plaques have been developed, initially in two or three dimensions and/or without a stent present [27, 33, 42, 49] to investigate stent-artery interactions. Pericevic et al. [51] performed the first scientific study to investigate the influence of plaque composition on underlying arterial wall stress during stent expansion using porcine artery mechanical properties. However, recent studies on stent-artery interaction in order to characterize the most vulnerable plaque during stenting have almost entirely used animal artery mechanical properties. The mechanical properties of animal coronary arteries are bounded value and can only be used for approximate estimation of cognate parameters in human. In addition, it has been indicated that the mechanical properties of human and porcine arteries are significantly different [24, 31] and, subsequently, the implementation of simplified animal artery mechanical properties might affect the induced stress value on the plaque, artery, and stent wall.

This study is aimed at determining the influence of plaque properties on the stresses induced within the arterial wall due to the implantation of a balloon expandable coronary stent inside a stenotic artery using a nonlinear finite element approach. To do this, human coronary arteries were removed from healthy and atherosclerotic individuals within 5 h postmortem. The samples were then subjected to a series of circumferential tensile tests. The Ogden hyperelastic material coefficients were computed using obtained stress-strain diagrams. The Ogden material coefficients were implemented into the FE model for further study. It is believed that the understanding of the stresses within the plaque tissues and arterial wall will provide a comprehensive knowledge as to which plaque tissue is more vulnerable to initiate the rupture. In addition, it will provide a valuable knowledge for plaque vulnerability assessment to minimize injury to the artery wall.

Materials and methods

Experimental procedures

The surgical and tensile test procedures have been comprehensively described in our previous studies [17, 24, 30–32]. Briefly, the coronary arteries were excised at autopsy from six male individuals. The coronary arteries were then stored in a solution of 0.90% w/v of NaCl in 4–5°C before the test begins to lessen tissue degradation. The coronary artery specimens were taken out from the physiological saline and subjected to a circumferential constant strain of 5 mm/min to obtain their stress-strain diagrams after preconditioning [12, 19, 20, 23, 35]. The use of human testing materials was approved by the Ethics Committee of the Legal Medicine Organization.

Model structure and mesh

A comparative three-dimensional numerical simulation of an idealized stent-plaque-artery interaction was developed to anticipate stress conditions within plaque, arterial wall, and stent during stent deployment for various plaque compositions. Three models were developed, each representing a plaque of different material composition, such as calcified, cellular, or hypocellular. The models were established, meshed, and solved using the explicit dynamics finite element code LS-DYNA 970 (LSTC, Livermore, CA, USA). The balloon, stent, plaque, and artery dimensions were obtained from the available studies [3, 14, 27, 33]. Briefly, the stent design used in the simulations was based on the 3.5 mm Driver stent (Medtronic, Minneapolis, MN, USA). The individual stent strut width was 0.1963 mm in the circumferential direction and the length of the bridging strut connecting between the two adjacent cells was 0.29 mm. The finite element model of the stent was meshed with brick elements to properly model the geometry. A polyurethane rubber type material was used to represent the balloon. The balloon as a medium to expand the stent was modeled to be 12 mm in length. The outer diameter of the balloon was 2.9 mm and the thickness of the balloon was 0.1 mm. The balloon was modeled using eight node three-dimensional explicit dynamic solid brick elements. By taking the advantage of symmetrical conditions, only a quarter of the stent and balloon was modeled. Symmetric boundary conditions were imposed on the nodes of the stent and balloon in the planes of symmetry where all the nodes perpendicular to the y-axis were not allowed to move in y-direction and all the nodes perpendicular to the x-axis were not allowed to move in x-direction. Both ends of the stent were free from any constraints so that the expansion and shortening behavior of the stent would be observed. For modeling purposes, the balloon was assumed to be fully tethered at both ends, and hence, only the expansion in a radial direction was permitted. An automatic surface-to-surface algorithm approach was selected in order to cope with the nonlinear contact problem between the two component surfaces. The inner diameter of the healthy artery and the stenotic plaque (middle section) was

4 mm and 2.5 mm, respectively. The artery on the outer side of the plaque was considered to consist of three tissue layers, including intima, media and adventitia, with a thickness of 0.10 mm, 0.20 mm and 0.20 mm, respectively. The interfaces between different artery layers were assumed to be coherent and treated as perfectly bonded, which is also the case for the interface between the artery wall and the stenotic plaque.

The pressure load was applied as a surface load on the inner surface of the balloon, expanding the stent radially past its elastic limit to a maximum diameter before failure stress was reached. The balloon was subjected to a uniform internal pressure increasing from 0 to 0.409 MPa at a constant rate of 1.635 ms. Ramp loading at an adequately slow rate that has small kinetic energy or small oscillations helps to find the relationship of pressure level to ultimate tensile strength of the stent material. In order to get rid of, or to diminish the dynamic effects, some analyses with different values of system damping coefficient were conducted. It was found that the system damping coefficient of ten triggers suitable results.

Material properties-constitutive equations

A bi-linear elasto-plastic material model was employed for the stent material. The material properties were chosen to approximately represent stainless steel 304. This material model accounts for the permanent stent deformation following expansion. Nonlinear analysis approach and a hyperelastic material model were chosen to represent the balloon. Two parameter Mooney-Rivlin model constants were derived using test data, which represents all modes of deformation and strain ranges that the model will experience [3].

The arterial wall and three types of plaque material (calcified, cellular, and hypocellular) [14, 22, 27] were defined by the Ogden hyperelastic constitutive equation. This has been found to adequately describe the nonlinear stress-strain relationship of elastic arterial tissue [14, 18, 39]. An isotropic material has the same mechanical response regardless of loading direction. For an isotropic hyperelastic material, the strain energy density function W is a scalar function of the right Cauchy-Green deformation tensor, C. The scalar function is composed of either the principal invariants or the principal stretches of the deformation, both of which are derived from the right Cauchy-Green deformation tensor [5, 13, 16, 21, 26]. The experimental data was used to calibrate an isotropic hyperelastic strain energy density function in order to generate stress-strain. Under the assumption that artery and plaque are nearly incompressible and isotropic materials [12, 30], it was possible to fit a general polynomial isotropic constitutive equation to form Eq. 1.

$$W=\sum_{i+j=1}^{N} C_{ij}(\bar{I}_1\text{-}3)^i(\bar{I}_2\text{-}3)^j+\sum_{i=1}^{N}\frac{1}{D_i}(J\text{-}1)^{2i}\vdots i,j=0,1,\ldots,N\vdots i+j=1,2,\ldots,N \quad (1)$$

In general, an isotropic hyperelastic incompressible material is characterized by a strain-energy density function W which is a function of two principal strain invariants only: $W=W(I_1, I_2)$, where I_1 and I_2 are defined as [15, 48]

$$I_1=\lambda_1^2+\lambda_2^2+\lambda_3^2 \quad (2)$$

$$I_2=\lambda_1^2\lambda_2^2+\lambda_1^2\lambda_3^2+\lambda_2^2\lambda_3^2 \quad (3)$$

Here, λ_1^2, λ_2^2, and λ_3^2 are the squares of the principal stretch ratios, linked by the relationship $\lambda_1\lambda_2\lambda_3=1$, due to incompressibility [28, 36].

Two different isotropic constitutive models were examined: Ogden (Eq. 4) and Mooney-Rivlin (Eq. 5). The Mooney-Rivlin [6, 14, 25, 29] models are special cases of the polynomial constitutive equations while the Ogden [7] can be also considered as a polynomial form in terms of the stretch ratios as its variables instead of the invariants. The polynomial along with the other specialized forms of the constitutive equations can be written as:

$$W=\sum_{i=1}^{N}\frac{\mu_i}{\alpha_i}(\bar{\lambda}_1^{\alpha_i}+\bar{\lambda}_2^{\alpha_i}+\bar{\lambda}_3^{\alpha_i}\text{-}3)+\sum_{i=1}^{N}\frac{1}{D_i}(J\text{-}1)^{2i} \quad (4)$$

$$W=C_{10}(\bar{I}_1\text{-}3)+C_{01}(\bar{I}_2\text{-}3)+\frac{1}{D_1}(J\text{-}1)^2 \quad (5)$$

where $J=det(F)$ and F is the deformation gradient. The terms, $\bar{I}_1$ and $\bar{I}_2$ are the first and second invariants, respectively, of the left Cauchy-Green strain tensor, $\bar{B}$. For a modified deformation gradient $\bar{F}=J^{-\frac{1}{3}}F$ the Cauchy-Green strain tensor assumes the form: $\bar{B}=\bar{F}\bar{F}^T$. The principal stretch, $\bar{\lambda}_i$ is the eigenvalue of $\bar{F}$ (deformation gradient) [34, 37]. The polynomial coefficients, μ_i, α_i, and C_{ij} are material constants that were fit from the experimental data.

The fully integrated artery-plaque-stent model was solved by a commercial explicit dynamics finite element code LS-DYNA 970 (LSTC). The hyperelastic material coefficients of arterial/plaque/balloon tissue and bilinear elasto-plastic model of stent are listed in Table 1. The Ogden and Mooney-Rivlin material coefficients for the human coronary artery tissues were calculated using a nonlinear least square fit optimization method, trust region algorithm. To do this, the materials coefficients were calibrated with experimental data provided by uniaxial tensile test.

Statistical analysis

Data were first analyzed by analysis of variance (ANOVA); when statistical differences were detected, student's t-test for comparisons between groups was performed using SPSS software version 16.0 (SPSS Inc., Chicago, IL, USA). Data are reported as mean±standard deviation at a significance level of $p<0.05$.

Results and discussion

Expanding a stent inside an artery will subject the plaque and artery to high stresses that can injure the tissue, potentially leading to further smooth muscle cell proliferation, neointimal hyperplasia and therefore in-stent restenosis. The level of stent-induced injury to the arterial tissue depends on a number of factors, such as the stent design, the geometry and curvature of the artery, the pressures to which the stent-delivery balloon is inflated, and the mechanical properties of the artery and plaque.

Table 1: The material coefficients of arterial tissue layers, plaque tissue, balloon, and stent.

Arterial tissue (Ogden)	μ_1 (MPa)	μ_2	μ_3	α_1	α_2	α_3
Healthy artery	0.431	-0.349	-0.032	8.317	8.311	-20.135
Atherosclerotic artery	0.830	0.651	-1.285	-13.818	12.719	-25.000
Arterial tissue (Mooney-Rivlin)	C_{10} (MPa)	C_{01}	C_{20}	C_{11}	C_{02}	–
Healthy artery	0.115	-0.049	1.403	-3.370	2.201	–
Atherosclerotic artery	1.574	-1.409	-14.347	38.065	-25.227	–
Plaque (Mooney-Rivlin)	μ_1 (MPa)	μ_2	μ_3	α_1	α_2	α_3
Calcified	-4.954	2.869	2.136	24.328	24.999	23.152
Cellular	7.280	-9.733	-2.245	-4.742	-1.792	-7.923
Hypocellular	-0.588	0.654	-0.048	12.452	12.451	-25
Balloon (Mooney-Rivlin)	C_{10} (MPa)	C_{01}	–	–	–	–
	1.031	3.69	–	–	–	–
Stent (Bi-linear elasto-plastic)	Young modulus (MPa)	Shear modulus	Tangent modulus	Yield strength	–	–
	193,000	75,000	692	207	–	–

The objective of this study was to determine the mechanical properties of healthy and atherosclerotic human coronary arteries (Figure 1). In addition, a further objective was to investigate the influence of artery and plaque type on the stresses induced in the plaque, arterial wall, and stent for the same stent geometry within an idealized model of a stenosed artery as presented in Figure 2. The distribution of von Mises stress in the plaques is shown in Figure 3 for calcified, cellular, and hypocellular plaque. In addition, the stress distribution in the expanded stents is indicated in Figure 4 for calcified, cellular, and hypocellular plaque. The symmetrical stress distributions around the central axis of artery prove the modeling and imposed boundary conditions. A comparative histogram representation of maximum stress on plaque and stent is demonstrated in Figure 5. The plaque type was observed to have a significant influence on the stresses induced within the artery during stenting. The results revealed that the highest stress occurred in a calcified plaque with 3.169 MPa. This stress for cellular and hypocellular plaque was 1.912 and 2.51 MPa, respectively (Figure 5A). It was also indicated that the highest stress occurred in the calcified plaque was high enough for fracture in this pretty brittle material [38]. Stress analysis showed non-significant differences on stents for different plaque types (Figure 5B). The von Mises stresses on the stents were found to be similar in all cases, in terms of both distribution and magnitude with <2% differences. However, the maximum von Mises stress on the calcified plaque is higher than that on the hypocellular plaque as compared in Figure 5A. Previous studies indicated the maximum stress of 249 MPa in stent [33]. This study, however, computed the maximum stress as a function of plaque types. A maximum von Mises stress on stent for calcified plaque was 1.57% and 1.33% higher than

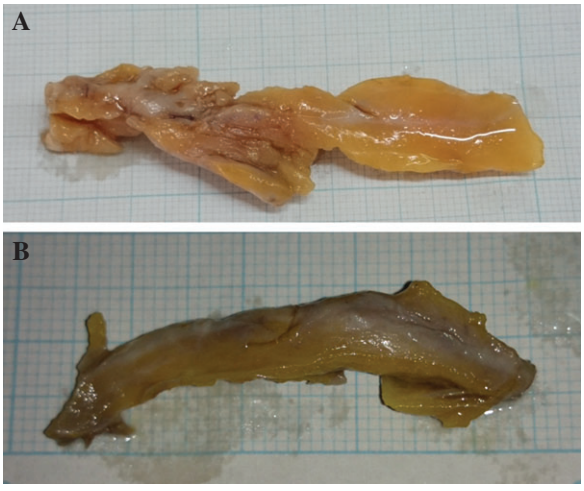

Figure 1: The (A) healthy and (B) atherosclerotic human coronary arteries.

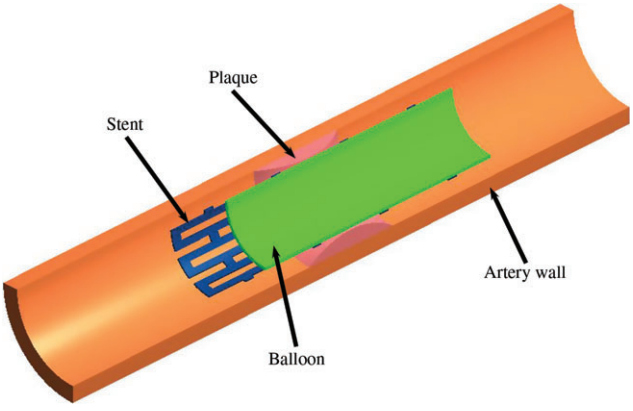

Figure 2: The finite element model of arterial wall, plaque, balloon, and stent.

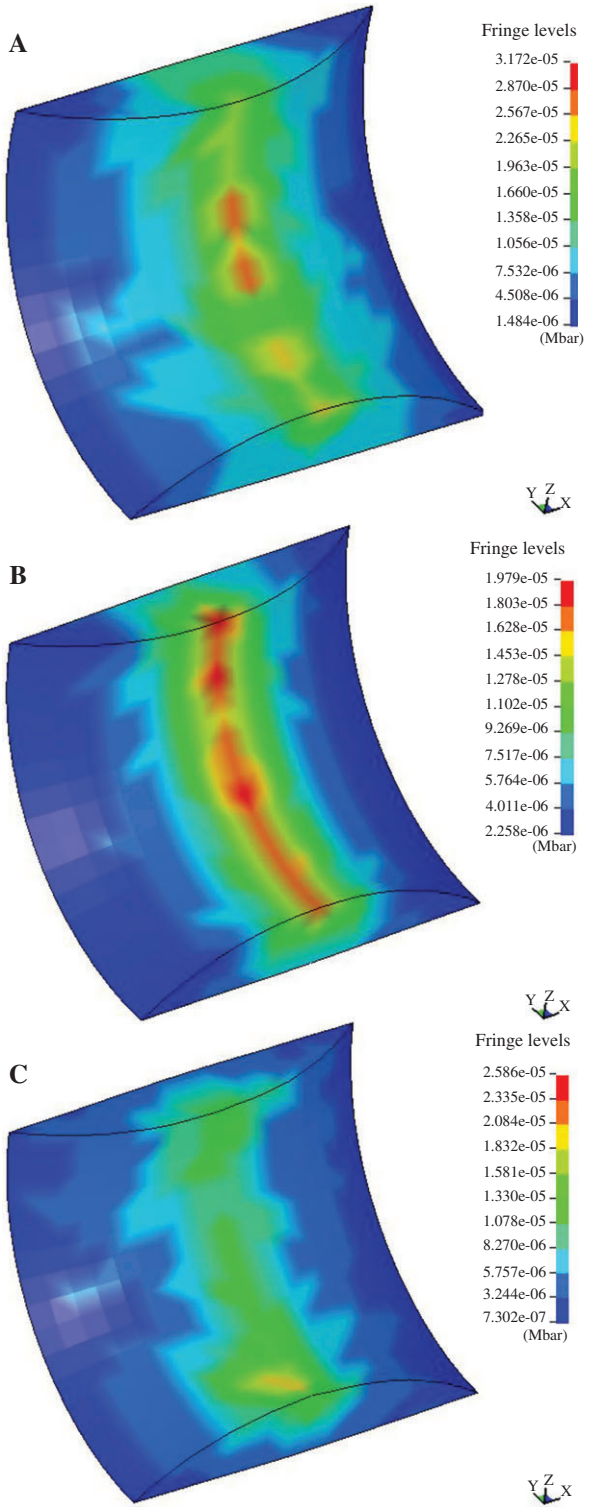

Figure 3: Stress distribution on plaque wall for (A) calcified, (B) cellular, and (C) hypocellular plaques. (Stresses are reported in Mbar).

that of cellular and hypocellular ones, respectively. The region of highest stresses is located at the four corners of the cells. This is related to the struts being pulled apart from each other to form a rhomboid shape of cells during the expansion. In most cases, the stress concentration tends to occur on the plaque due to the direct contact of the plaque with the expanded stent. The central radial displacement of the plaque and arterial walls during stent expansion is predicted to depend on the plaque type. The stress-strain diagram of the plaque tissues is plotted in Figure 6A. The calcified and cellular plaques were observed to have almost same mechanical behavior, whereas the lowest stress was seen for hypocellular plaque. The stress for an arbitrary element on the arterial wall was computed for arterial wall injury assessment. A comparative stress-strain diagram of the arterial wall under radial loading for calcified, cellular, and hypocellular plaque is presented in Figure 6B. In addition, a comparative histogram representation of maximum stress on the arterial wall for calcified, cellular, and hypocellular plaques were computed and presented in Figure 7. The stresses on the arterial wall with calcified and cellular plaques were predicted to be relatively low, while the highest computed stresses was seen to be located on the arterial wall with hypocellular plaque. These results suggest that the arterial wall with hypocellular plaque is prone to rupture, whereas the arterial wall with calcified and cellular plaque play a protective role. After deflation, the maximum stress shifted to the plaque, especially at locations where the stent and the plaque are in full contact. Regarding the stress on the arterial wall, the highest stress was observed with the hypocellular plaque (448 kPa), while the lowest stress was seen with the calcified plaque (100 kPa). The reason is that the calcified plaque is much stiffer and more resistant to stretch than the hypocellular plaque, which prohibited the effective expansion of the stent-artery system.

The predicted stress levels were used to estimate the minimum and maximum percentage of plaque tissue that might rupture during stent deployment in the given artery as a function of plaque type. The risk of arterial damage and/or rupture is higher for hypocellular plaque, as calcified and cellular plaques show considerable load-bearing abilities that diminish the stresses within the arterial tissue layers. Based on reported values of stress at calcified plaque fracture [10, 44], fracture is anticipated to happen in calcified plaques regardless of stent inflation pressures. Available fracture data [44] for different plaque types suggest that rupture may occur over a large range of stress values. From this data, the critical stress range was taken to be 160–700 kPa for the calcified plaque tissue, 300–640 kPa for the cellular tissue, and 550 KPa for the hypocellular tissue. Our results predicted the stress values of 2.38, 1.91, and 1.59 MPa for calcified,

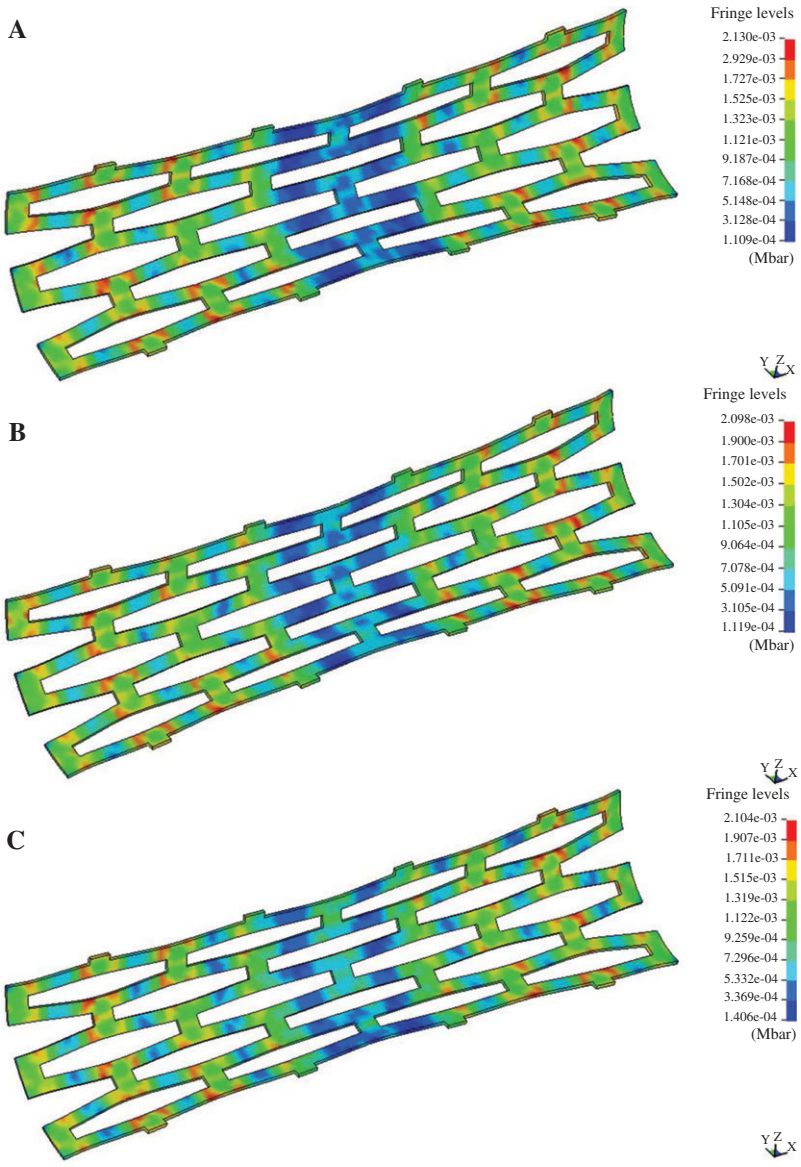

Figure 4: Stress distribution on stent for (A) calcified, (B) cellular, and (C) hypocellular plaques. (Stresses are reported in Mbar).

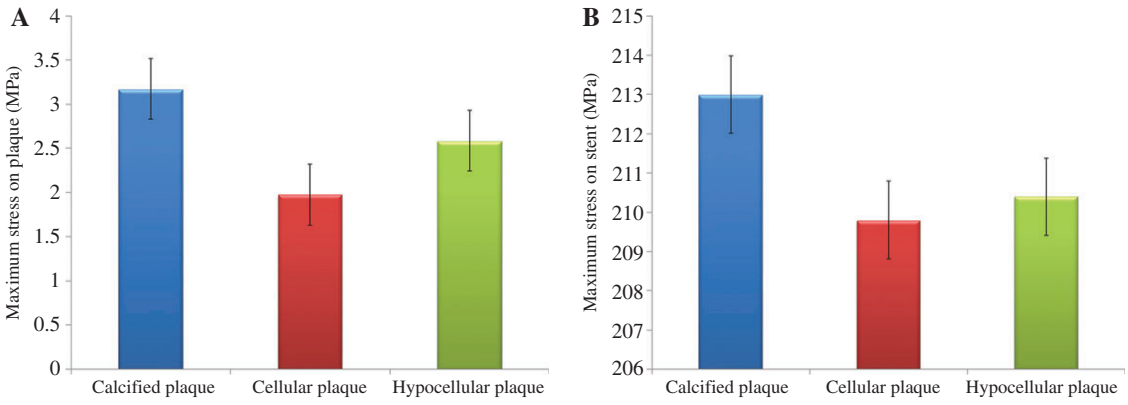

Figure 5: A comparative histogram representation of maximum stress on (A) plaque wall and (B) stent for calcified, cellular, and hypocellular plaques.

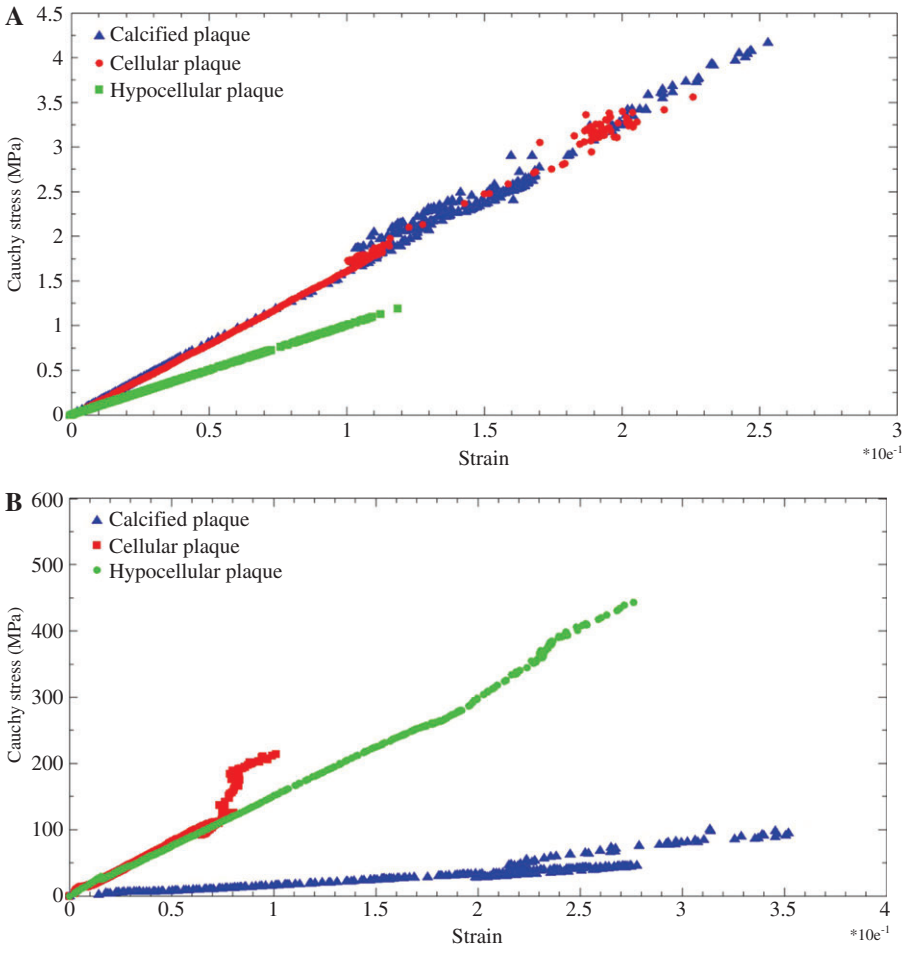

Figure 6: The stress-strain diagrams of (A) different plaques and (B) arterial tissue during stent expansion inside a stenotic artery.

cellular, and hypocellular, respectively. These results suggest that the risk of plaque rupture almost equal for all plaque types with a relatively higher risk for calcified plaque owing to a considerable difference from its critical range. Considering a lower rupture stress for calcified tissue (160 kPa), it seems that the risk of failure and/or embolisis is highest for this plaque type. As a result of the highest stiffness of calcified plaque compared to cellular and hypocellular plaques, the highest stress on arterial wall may occur [44]. Pericevic et al. [51] indicated that higher stresses occurred in the artery wall for cellular and hypocellular plaques, while the stiffer calcified plaque appeared to play a protective role. Our results indeed suggest that higher pressure can be applied to calcified plaques with a lower risk of arterial vascular injury. The results also suggest the need for the design of artery and lesion specific stents, where imaging techniques, such as intravascular ultrasound [9] or high-resolution magnetic resonance imaging [40, 45], are used to determine plaque composition prior to angioplasty and stenting.

Limitations

Although the present study tried to investigate the vulnerability within arterial and plaque tissues using nonlinear FE analysis, there are some simplifications that should

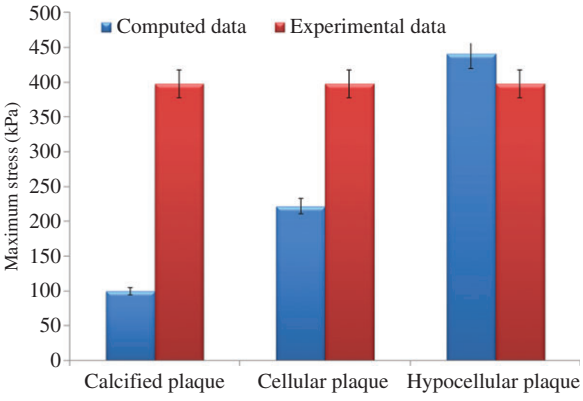

Figure 7: A comparative histogram representation of computed and experimental maximum stress data in the arterial wall for calcified, cellular, and hypocellular plaques.

be improved in future studies. In the present model, the nonlinear nature of arterial plaques was accounted by the application of the Ogden hyperelastic constitutive model. All tissues, including artery and plaque were assumed incompressible, isotropic, and homogenous. However, atherosclerotic plaques have been shown to be heterogeneous [53], viscoelastic [52], or perhaps visco-hyperelastic. Accessing atherosclerotic type-specific differences in the structure and mechanical properties of different tissue components in plaques will be an important development for future finite element models of stent-artery interactions. An idealized artery and plaque geometry was also assumed in the current analyses. Despite these simplifications, the present model demonstrates the importance of the plaque type in terms of the potential injury to a stented artery, injury that may have significant implications for in-stent restenosis, balloon angioplasty, and stenting.

Conclusions

In this study, an experimental work was conducted to measure the stress-strain diagram of healthy and atherosclerotic human coronary arteries. Afterwards, the Ogden and Mooney-Rivlin material coefficients of healthy and atherosclerotic arteries were determined. The parameters of the Ogden material model were implemented into the FE model to analyze the influence on plaque types (calcified, cellular, and hypocellular) on plaque, arterial wall, and stent stresses during the implantation of the intracoronary balloon expandable stent. The results revealed a significant influence of plaque types on the stresses induced within the plaque and arterial wall during stenting but not when calculating the maximum von Mises stress on stent. Higher stresses were observed in the plaque wall for stiffer calcified plaque, whilst the cellular and hypocellular plaques showed less stress on their wall. The results also revealed that the highest computed von Mises stresses were located on the arterial wall with hypocellular plaque, whilst the arterial walls with calcified and cellular plaques played a protective role. These models can be used to determine the influence of artery and plaque properties on both the initial lumen gain achieved following stenting, as well as estimating the level of artery wall injury. Therefore, they can provide valuable clinical indicators in stenting various atherosclerotic lesions.

Acknowledgments: The authors acknowledge the Iran University of Science and Technology for funding this project.

Conflicts of interest statement: The authors declare that they have no conflicts of interest.

References

[1] Chua S, Mac Donald B, Hashmi M. Finite-element simulation of stent expansion. J Mater Process Tech 2002; 120: 335–340.
[2] Colombo A, Stankovic G, Moses JW. Selection of coronary stents. J Am Coll Cardiol 2002; 40: 1021–1033.
[3] David Chua SN, Mac Donald BJ, Hashmi MSJ. Finite element simulation of stent and balloon interaction. J Mater Process Tech 2003; 143–144: 591–597.
[4] de Weert TT, Ouhlous M, Zondervan PE, et al. In vitro characterization of atherosclerotic carotid plaque with multidetector computed tomography and histopathological correlation. Eur Radiol 2005; 15: 1906–1914.
[5] Faghihi S, Gheysour M, Karimi A, Salarian R. Fabrication and mechanical characterization of graphene oxide-reinforced poly (acrylic acid)/gelatin composite hydrogels. J Appl Phys 2014; 115: 83513–83520.
[6] Faghihi S, Karimi A, Jamadi M, Imani R, Salarian R. Graphene oxide/poly(acrylic acid)/gelatin nanocomposite hydrogel: Experimental and numerical validation of hyperelastic model. Mater Sci Eng: C 2014; 38: 299–305.
[7] Faturechi R, Karimi A, Hashemi A, Navidbakhsh M. Mechanical characterization of Peritoneum/Fascia under uniaxial loading. J Biomater Tissue Eng 2014; 4: 189–193.
[8] Halabian M, Karimi A, Barati E, Navidbakhsh M. Numerical evaluation of stenosis location effects on hemodynamics and shear stress through curved artery. J Biomater Tissue Eng 2014; 4: 349–357.
[9] Hamilton AJ, Kim H, Nagaraj A, et al. Regional material property alterations in porcine femoral arteries with atheroma development. J Biomech 2005; 38: 2354–2364.
[10] Holzapfel GA, Sommer G, Regitnig P. Anisotropic mechanical properties of tissue components in human atherosclerotic plaques. J Biomech Eng 2004; 126: 657–665.
[11] Holzapfel GA, Stadler M, Gasser TC. Changes in the mechanical environment of stenotic arteries during interaction with stents: computational assessment of parametric stent designs. J Biomech Eng 2005; 127: 166–180.
[12] Karimi A, Navidbakhsh M. Measurement of the nonlinear mechanical properties of a poly (vinyl alcohol) sponge under longitudinal and circumferential loading. J Appl Polym Sci 2013; 131: 40257–40264.
[13] Karimi A, Navidbakhsh M. An experimental study on the mechanical properties of rat brain tissue using different stress-strain definitions. J Mater Sci Mater Med 2014; 25: 1623–1630.
[14] Karimi A, Navidbakhsh M. A comparative study on the uniaxial mechanical properties of the umbilical vein and umbilical artery using different stress–strain definitions. Australas Phys Eng Sci Med 2014; 37: 645–654.
[15] Karimi A, Navidbakhsh M. Constitutive model for numerical analysis of polyvinyl alcohol sponge under different strain rates. J Thermoplastic Composite Mater 2014. Doi: 10.1177/0892705713520176.

[16] Karimi A, Faturechi R, Navidbakhsh M, Hashemi A. A nonlinear hyperelastic behavior to identify the mechanical properties of rat skin under uniaxial loading. J Mech Med Biol 2014; 5: 1450075–1450089.
[17] Karimi A, Navidbakhsh M, Alizadeh M, Razaghi R. A comparative study on the elastic modulus of polyvinyl alcohol sponge using different stress-strain definitions. Biomed Tech (Berl) 2014; 59: 439–446.
[18] Karimi A, Navidbakhsh M, Alizadeh M, Shojaei A. A comparative study on the mechanical properties of the umbilical vein and umbilical artery under uniaxial loading. Artery Res 2014; 8: 51–56.
[19] Karimi A, Navidbakhsh M, Beigzadeh B. A visco-hyperelastic constitutive approach for modeling polyvinyl alcohol sponge. Tissue Cell 2014; 46: 97–102.
[20] Karimi A, Navidbakhsh M, Beigzadeh B, Faghihi S. Hyperelastic mechanical behavior of rat brain infected by Plasmodium berghei ANKA-Experimental testing and constitutive modeling. Int J Damage Mech 2014; 23: 857–871.
[21] Karimi A, Navidbakhsh M, Faghihi S. Measurement of the mechanical failure of PVA sponge using biaxial puncture test. J Biomater Tissue Eng 2014; 4: 46–50.
[22] Karimi A, Navidbakhsh M, Faghihi S. A comparative study on plaque vulnerability using constitutive equations. Perfusion 2014; 29: 179–184.
[23] Karimi A, Navidbakhsh M, Faghihi S. Fabrication and mechanical characterization of a polyvinyl alcohol sponge for tissue engineering applications. Perfusion 2014; 29: 231–237.
[24] Karimi A, Navidbakhsh M, Faghihi S, Shojaei A, Hassani K. A finite element investigation on plaque vulnerability in realistic healthy and atherosclerotic human coronary arteries. Proc IMech Eng Part H 2013; 227: 148–161.
[25] Karimi A, Navidbakhsh M, Motevalli Haghi A, Faghihi S. Measurement of the uniaxial mechanical properties of rat brains infected by Plasmodium berghei ANKA. Proc IMech Eng Part H 2013; 227: 609–614.
[26] Karimi A, Navidbakhsh M, Razaghi R. An experimental-finite element analysis on the kinetic energy absorption capacity of polyvinyl alcohol sponge. Mater Sci Eng: C 2014; 39: 253–258.
[27] Karimi A, Navidbakhsh M, Razaghi R. Plaque and arterial vulnerability investigation in a three-layer atherosclerotic human coronary artery using computational fluid-structure interaction method. J Appl Phys 2014; 116: 064701–064710.
[28] Karimi A, Navidbakhsh M, Razaghi R. Dynamic finite element simulation of the human head damage mechanics protected by polyvinyl alcohol sponge. Int J Damage Mech 2014. Doi: 10.1177/1056789514535945.
[29] Karimi A, Navidbakhsh M, Razaghi R, Haghpanahi M. A computational fluid-structure interaction model for plaque vulnerability assessment in atherosclerotic human coronary arteries. J Appl Phys 2014; 115: 144702–144711.
[30] Karimi A, Navidbakhsh M, Rezaee T, Hassani K. Measurement of the circumferential mechanical properties of the umbilical vein: experimental and numerical analyses. Comput Methods Biomech Biomed Eng 2015; 18: 1418–1426.
[31] Karimi A, Navidbakhsh M, Shojaei A, Faghihi S. Measurement of the uniaxial mechanical properties of healthy and atherosclerotic human coronary arteries. Mater Sci Eng C 2013; 33: 2550–2554.
[32] Karimi A, Navidbakhsh M, Shojaei A, Hassani K, Faghihi S. Study of plaque vulnerability in coronary artery using Mooney-Rivlin model: A combination of finite element and experimental method. Biomed Eng Appl Basis Commun 2013; 26: 145–152.
[33] Karimi A, Navidbakhsh M, Yamada H, Razaghi R. A nonlinear finite element simulation of balloon expandable stent for assessment of plaque vulnerability inside a stenotic artery. Med Biol Eng Comput 2014; 52: 589–599.
[34] Karimi A, Navidbakhsh M, Yamada H, Rezaee T, Hassani K. A comparative study on the quasilinear viscoelastic mechanical properties of umbilical artery and umbilical vein. Perfusion 2014. Doi: 0267659114536761.
[35] Karimi A, Navidbakhsh M, Yousefi H. Mechanical properties of polyvinyl alcohol sponge under different strain rates. Int J Mater Res 2014; 105: 404–408.
[36] Karimi A, Navidbakhsh M, Yousefi H, Alizadeh M. An experimental study on the elastic modulus of gelatin hydrogel using different stress-strain definitions. J Thermoplastic Composite Mater 2014. Doi: 10.1177/0892705714533377.
[37] Karimi A, Navidbakhsh M, Yousefi H, Motevalli Haghi A, Adnani Sadati SJ. Experimental and numerical study on the mechanical behavior of rat brain tissue. Perfusion 2014; 29: 307–314.
[38] Lally C, Dolan F, Prendergast P. Cardiovascular stent design and vessel stresses: a finite element analysis. J Biomech 2005; 38: 1574–1581.
[39] Lally C, Reid A, Prendergast P. Elastic behavior of porcine coronary artery tissue under uniaxial and equibiaxial tension. Ann Biomed Eng 2004; 32: 1355–1364.
[40] LaMuraglia GM, Southern JF, Fuster V, Kantor HL. Magnetic resonance images lipid, fibrous, calcified, hemorrhagic, and thrombotic components of human atherosclerosis in vivo. Circulation 1996; 94: 932–938.
[41] Lee RT, Grodzinsky AJ, Frank EH, Kamm RD, Schoen FJ. Structure-dependent dynamic mechanical behavior of fibrous caps from human atherosclerotic plaques. Circulation 1991; 83: 1764–1770.
[42] Li Z-Y, Howarth S, Trivedi RA. Stress analysis of carotid plaque rupture based on in vivo high resolution MRI. J Biomech 2006; 39: 2611–2622.
[43] Liang D, Yang D, Qi M, Wang W. Finite element analysis of the implantation of a balloon-expandable stent in a stenosed artery. Int J Cardiol 2005; 104: 314–318.
[44] Loree HM, Grodzinsky AJ, Park SY, Gibson LJ, Lee RT. Static circumferential tangential modulus of human atherosclerotic tissue. J Biomech 1994; 27: 195–204.
[45] Martin AJ, Gotlieb AI, Henkelman RM. High resolution MR imaging of human arteries. J Magn Reson Im 1995; 5: 93–100.
[46] Naghavi M, Libby P, Falk E, et al. From vulnerable plaque to vulnerable patient a call for new definitions and risk assessment strategies: part I. Circulation 2003; 108: 1664–1672.
[47] Nair A, Kuban BD, Tuzcu EM, Schoenhagen P, Nissen SE, Vince DG. Coronary plaque classification with intravascular ultrasound radiofrequency data analysis. Circulation 2002; 106: 2200–2206.
[48] Ogden RW. Non-linear elastic deformations. New York: Dover 1997.
[49] Ohayon J, Teppaz P, Finet G, Rioufol G. In-vivo prediction of human coronary plaque rupture location using intravascular

ultrasound and the finite element method. Coronary Artery Dis 2001; 12: 655–663.
[50] Palmaz JC. Intravascular stenting: from basic research to clinical application. Cardiovasc Inter Radiol 1992; 15: 279–284.
[51] Pericevic I, Lally C, Toner D, Kelly DJ. The influence of plaque composition on underlying arterial wall stress during stent expansion: the case for lesion-specific stents. Med Eng Phys 2009; 31: 428–433.
[52] Salunke N, Topoleski L, Humphrey J, Mergner W. Compressive stress relaxation of human atherosclerotic plaque. J Biomed Mater Res 2001; 55: 236–241.
[53] Topoleski L, Salunke N, Humphrey J, Mergner W. Composition and history dependent radial compressive behavior of human atherosclerotic plaque. J Biomed Mater Res 1997; 35: 117–127.
[54] Wang W-Q, Liang D-K, Yang D-Z, Qi M. Analysis of the transient expansion behavior and design optimization of coronary stents by finite element method. J Biomech 2006; 39: 21–32.